JVSTB
JOURNAL OF VACUUM SCIENCE AND TECHNOLOGY B

Developer-free direct patterning of PMMA/ZEP 520A by low voltage electron beam lithography

David Ai Zhi Zheng, Mohammad Ali Mohammad, Steven Kelly Dew, and Maria Stepanova

Citation: J. Vac. Sci. Technol. B **29**, 06F303 (2011); doi: 10.1116/1.3634017
View online: http://dx.doi.org/10.1116/1.3634017
View Table of Contents: http://avspublications.org/resource/1/JVTBD9/v29/i6
Published by the AVS: Science & Technology of Materials, Interfaces, and Processing

Related Articles

Negative electron-beam resist hard mask ion beam etching process for the fabrication of nanoscale magnetic tunnel junctions
J. Vac. Sci. Technol. B 30, 06FA01 (2012)

Long nanoscale gaps on III–V substrates by electron beam lithography
J. Vac. Sci. Technol. B 30, 06F305 (2012)

Fabrication of on-chip fluidic channels incorporating nanopores using self-aligned double layer resist processing technique
J. Vac. Sci. Technol. B 30, 06F802 (2012)

Control of inclination angle of glass-like carbon mold by defocus UV exposure on Si-containing photoresist
J. Vac. Sci. Technol. B 30, 06FB12 (2012)

Sub-30nm pitch line-space patterning of semiconductor and dielectric materials using directed self-assembly
J. Vac. Sci. Technol. B 30, 06F205 (2012)

Additional information on J. Vac. Sci. Technol. B

Journal Homepage: http://avspublications.org/jvstb
Journal Information: http://avspublications.org/jvstb/about/about_the_journal
Top downloads: http://avspublications.org/jvstb/top_20_most_downloaded
Information for Authors: http://avspublications.org/jvstb/authors/information_for_contributors

ADVERTISEMENT

Developer-free direct patterning of PMMA/ZEP 520A by low voltage electron beam lithography

David Ai Zhi Zheng (鄭愛智), Mohammad Ali Mohammad, and Steven Kelly Dew
Department of Electrical and Computer Engineering, University of Alberta, Edmonton, Alberta T6G 2V4, Canada

Maria Stepanova[a)]
National Institute for Nanotechnology NRC, Edmonton, Alberta T6G 2M9, Canada, and Department of Electrical and Computer Engineering, University of Alberta, Edmonton, Alberta, T6G 2V4, Canada

(Received 22 June 2011; accepted 15 August 2011; published 9 September 2011)

The authors report an approach that has potential to fabricate dense structures without liquid development. Two kinds of positive tone electron beam resist, 950k PMMA and ZEP 520A (Nippon Zeon), were studied for their properties and behaviors while subjecting them to exposure, thermal development, and reactive ion etching. So far, we have successfully patterned 70 nm half-pitch gratings in both 950k PMMA and ZEP 520A without liquid development. © *2011 American Vacuum Society*. [DOI: 10.1116/1.3634017]

I. INTRODUCTION

In conventional positive tone electron beam lithography (EBL) processing, liquid developers are used to remove exposed resist through the dissolution of more soluble fragments. However, liquid development introduces challenges such as optimization of developer formulation, time, temperature, etc. In addition, dense structure definition is limited by factors such as resist swelling and capillary force induced pattern collapse. Hence, a simplified development process that avoids liquid development could be quite attractive for EBL patterning of dense structures.

Recent studies by Koop *et al.*[1] showed that PMMA exhibits shrinkage after the electron beam exposure. Similar observations have also been reported by Kotera and Akiba.[2] Possible mechanisms for this effect include electron beam evaporation of resist or residual solvent, formation of volatile species through polymer fragmentation, and resist densification. Although relatively minor, this thickness reduction during electron exposure suggests a pathway for avoiding liquid development. In this work, we explore exposure conditions to see if the thickness reduction can be made more pronounced. We further consider postexposure dry processing to extend the effect.

The experiments by Koop *et al.*[1] and Kotera and Akiba[2] were conducted at relatively high energies between 20 and 30 keV. We believe that electron-resist interactions are enhanced at lower energies due to the higher collision cross section. This suggests that exposure energy could be an important factor in thickness reduction. Further, if electron induced fragmentation produces more volatile fragments, then postexposure heating[3] should enhance this effect. Even partial thickness reduction could be sufficient, if anisotropic reactive ion etching (RIE)[4–6] can preserve the height difference, whereas the thinner resist areas are etched to clearance. If successful, we will have a technique that greatly simplifies nanoscale dense structure patterning by eliminating the liquid development stage and its associated problems.

In this work, we have studied the effect of exposure dose, energy and initial film thickness on resist thickness reduction during exposure. We have further examined the effect of postexposure heating and RIE as strategies to assess the viability of a development procedure that avoids the use of liquids. We have focused on popular positive tone PMMA and ZEP (Nippon Zeon) resists. We have employed atomic force microscopy (AFM) and scanning electron microscopy (SEM) for assessing the effectiveness of this approach.

II. EXPERIMENT

A. Common sample preparations

The resists used were standard 950k PMMA (1%–2%) from MicroChem Corp and ZEP 520A (ZEP:Anisole = 1:3) from Zeon Chemicals LP on silicon wafers (100). PMMA samples were prebaked at 150 °C for 5 min on a hot plate and ZEP samples were prebaked at 170 °C for 10 min on a hot plate. Different film thicknesses were obtained by varying spin-on conditions and measured by ellipsometry. Most exposures were done at 3 keV and 10 μm aperture in a Raith 150 EBL system unless otherwise noted. An array of 1 μm^2 squares was chosen as our standard test structure because of its ease for AFM inspection and results calculation. Grating structures down to 50 nm half-pitch were also assessed using SEM.

B. Data acquisition by AFM

We have used two functions, bearing analysis and section analysis, of a Veeco Dimension 3100 AFM to extract height difference information and film thickness reduction information after electron beam irradiation. Bearing analysis was used to create a histogram that gave a distribution of depth at all sampled points on the surface with zero being the highest point. Therefore, the difference between the two distribution peaks is the height difference between exposed and

[a)]Electronic mail: Maria.Stepanova@nrc-cnrc.gc.ca

unexposed areas. Section analysis was used to confirm the bearing results along a single scan line. This provided a cross-sectional view of exposed pattern so that pattern distortions can be observed. Figure 1 is an example of how we have studied the dependency of various experimental parameters. The sample in this experiment was 63 nm thick 950k PMMA on Si exposed at 3 keV with the dose of 600 μC/cm^2. Figure 1(a) is a flattened top-view image with the height reference bar on the side. We can get a rough estimate of height difference from the top view and also observe the surface roughness. Figure 1(b) is the bearing analysis. As mentioned previously, the difference between the two peaks is the height difference between exposed and unexposed areas and this value is denoted by ΔT in our experiments. For this particular example ΔT is 20 nm, which is about 32% of the initial film thickness. Figure 1(c) is the section analysis. In addition to inspecting the height differences of individual or average cross sections, we can also observe the change of linewidth, line edge roughness, surface roughness, and other distortions.

C. Exposure dependency

We started our investigations with dependency studies of exposure dose, energy, and initial film thickness for ΔT and etch efficiency η. ΔT is the raw height difference between exposed and unexposed areas. The etch efficiency η is a parameter used to describe how efficient the electron beam is in reducing the film thickness per unit dose.

To determine dose dependency, a series of samples with constant resist thickness were exposed at the same energy but with varying doses. The detailed experimental conditions are given in the section of dose dependencies in Table I. To study energy dependency, a series of samples were exposed at various energies with the doses scaled proportionally to the energy to account for the normal variation in sensitivity.[7,8] The detailed experimental conditions are given in the section of energy dependencies in Table I. The reported dose factor shows the relative dose compared to the nominal dose scaled linearly with energy to the 1 keV reference condition. Finally, the effect of initial film thickness on ΔT was considered. The detailed experimental conditions are given in the "Initial Film Thickness Dependencies (PMMA)" section in Table I.

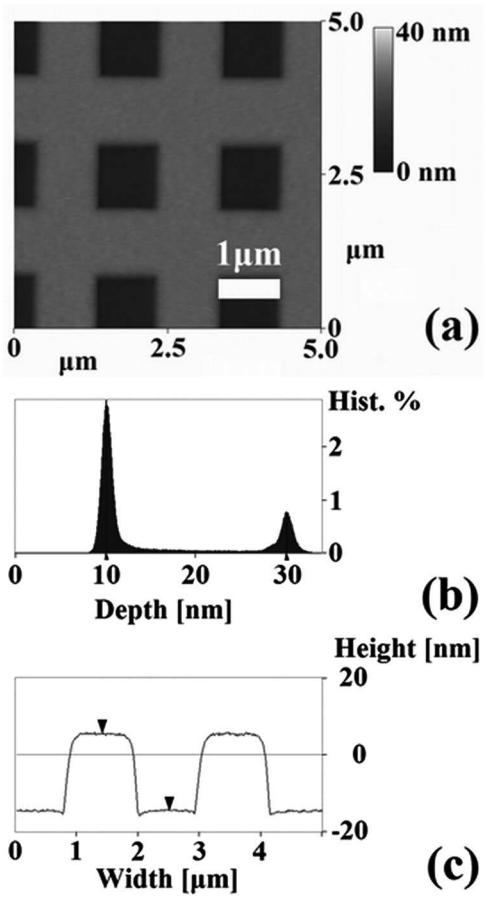

FIG. 1. AFM images of 63 nm 950k PMMA on Si, exposed at 3 keV at 600 μC/cm^2, without development. (a) Flattened top view; (b) bearing analysis; and (c) section analysis.

D. Postexposure processing

Following exposure, some samples were baked on a hot plate. Detailed heating conditions are given in Table II. For the heating experiments, we have also included ZEP samples. Temperatures ranged from 47.5 to 282 °C. Note that the glass transition temperatures for PMMA and ZEP are nominally 125 and 105 °C, respectively, although these may have been altered by conditions and processing.

TABLE I. Experimental conditions for dose, energy, and initial film thickness dependency studies.

Thickness (nm)	Aperture (μm)	Energy (keV)	Dose (μC/cm^2)	Factor[a]	ΔT (nm)
Dose dependencies (PMMA)					
63	10	1	33	1	2.9
63	10	1	66	2	5.5
63	10	1	132	4	10.4
63	10	1	198	6	14
63	10	3	100	1	6
63	10	3	200	2	11
63	10	3	400	4	18
63	10	3	600	6	20
Energy dependencies (PMMA)					
63	10	1	73.3	1	6.1
61	10	5	366.5	1	11.6
63	10	10	733.0	1	9.5
61	10	20	1,466.0	1	8
63	10	30	2,199.0	1	8.9
Initial film thickness dependencies (PMMA)					
31	10	3	400	4	9.7
63	10	3	400	4	18
131	20	3	400	4	32.9
31	10	3	600	6	10.9
63	10	3	600	6	20
131	20	3	600	6	37.4

[a]Factor refers to dose factor as doses are normalized to the base dose at each energy level.

TABLE II. Experimental conditions for heating dependency studies.

Thickness (nm)	Aperture (μm)	Energy (keV)	Dose (μC/cm^2)	Factor[a]	Heating	ΔT (nm)
PMMA (glass transition temperature is between 85 and 165 °C)						
31	10	3	400	4	N/A	9.5
31	10	3	600	6	N/A	10.6
31	10	3	800	8	N/A	11.8
31	10	3	1000	10	N/A	11.3
35	10	3	100	1	47.5 °C for 1min	N/A
35	10	3	200	2	47.5 °C for 1min	6.5
35	10	3	400	4	47.5 °C for 1min	8.1
35	10	3	600	6	47.5 °C for 1min	11.1
35	10	3	100	1	105 °C for 1min	10.7
35	10	3	200	2	105 °C for 1min	23.3
35	10	3	400	4	105 °C for 1min	27.7
35	10	3	600	6	105 °C for 1min	21.1
31	10	3	400	4	282 °C for 30min	19.5
31	10	3	600	6	282 °C for 30min	18.5
31	10	3	800	8	282 °C for 30min	17.5
31	10	3	1,000	10	282 °C for 30min	15.4
ZEP (glass transition temperature is 105 °C)						
78	10	3	50	2	N/A	4
78	10	3	100	4	N/A	6
78	10	3	150	6	N/A	8.2
78	10	3	200	8	N/A	10.2
78	10	3	50	2	75 °C for 30s	4
78	10	3	100	4	75 °C for 30s	10.6
78	10	3	150	6	75 °C for 30s	18.2
78	10	3	200	8	75 °C for 30s	20.8
78	10	3	50	2	100 °C for 1min	18.9
78	10	3	100	4	100 °C for 1min	37.9
78	10	3	150	6	100 °C for 1min	42
78	10	3	200	8	100 °C for 1min	44

[a]Factor refers to dose factor as doses are normalized to the base dose at each energy level.

In addition, some samples went through a RIE process after exposure. Our cryo-etch process was carried out by an Oxford Plasmalab System 100—ICP 180 at −110 °C. Descum conditions were 5 mTorr, $O_2 = 20$ sccm, ICP = 150 W, and rf = 20 W. Etching conditions were 7.5 mTorr, SF_6:$O_2 = 45$:10 sccm, ICP = 400 W, and rf = 6 W. The sample shown in the forthcoming Fig. 7 was 106 nm thick, 950k PMMA on Si, exposed at 3 keV, 1000 μC/cm^2. Following the exposure, the sample was introduced to the cryo-etch process, which included a 5 s de-scum and four 15 s etches. The sample was taken out for inspection of film thickness after each 15 s etch. The results shown in upcoming Fig. 8 were from a sample that was 131 nm thick, 950k PMMA on Si, exposed at 3 keV, 200–1000 μC/cm^2. Then the sample went through a cryo-etch of 10 s de-scum followed by a 60 s etch and then another 10 s de-scum followed by a 30 s etch. The sample was taken out for inspection of film thickness before the second de-scum and after the second etch. We have also tested a normal RIE process with a Trion Phantom RIE system. The sample was prepared and exposed under the same conditions as the sample shown in Fig. 7. Then the sample went through a normal RIE process at room temperature (~23 °C). RIE conditions were 50 mTorr, $O_2 = 10$ sccm, rf = 20 W for 30 s and then rf = 10 W for 45 s.

E. High resolution trials

The standard test structures we have used for the above-mentioned experiments were relatively big (1 μm^2 squares) so that both AFM inspections and calculations can be easily done. However, we have managed to pattern dense high resolution gratings on both PMMA and ZEP samples without liquid development or postexposure processing. Both PMMA and ZEP samples were exposed at 3 keV with 7.5 μm aperture. The gratings were 50 or 70 nm half-pitch for both resists. The film thickness for the PMMA sample was 72 nm, and for the ZEP sample, it was 64 nm. The dose range of the PMMA sample was from 100 to 900 μC/cm^2 and the ZEP sample was from 25 to 225 μC/cm^2.

III. RESULTS AND DISCUSSION

A. Exposure dependency

To help understand the results in the following sections, we defined an etch efficiency η (mm^3/C) to describe how effective the electron beam is in reducing the film thickness per unit dose. Hence, η equals to ΔT divided by area dose. We first studied the dose dependencies for thickness reduction of PMMA. The results are shown in Fig. 2 and clearly

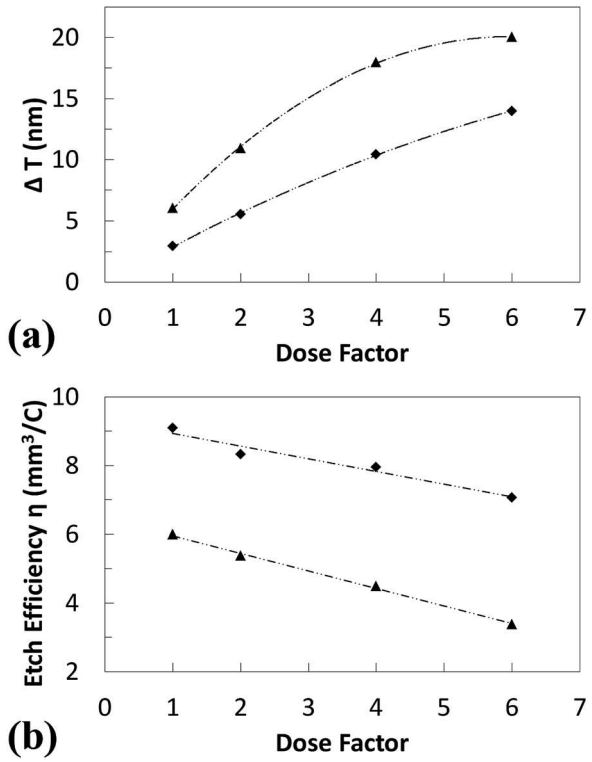

FIG. 2. Dose dependencies of (a) ΔT and (b) etch efficiency η. Sample was 63 nm 950k PMMA on Si, exposed at 3 keV with no development. Diamonds: 1 keV base dose = 33 μC/cm^2; triangles: 3 keV base dose = 100 μC/cm^2. Note: Dose factors are doses that normalized to the base dose at each energy level.

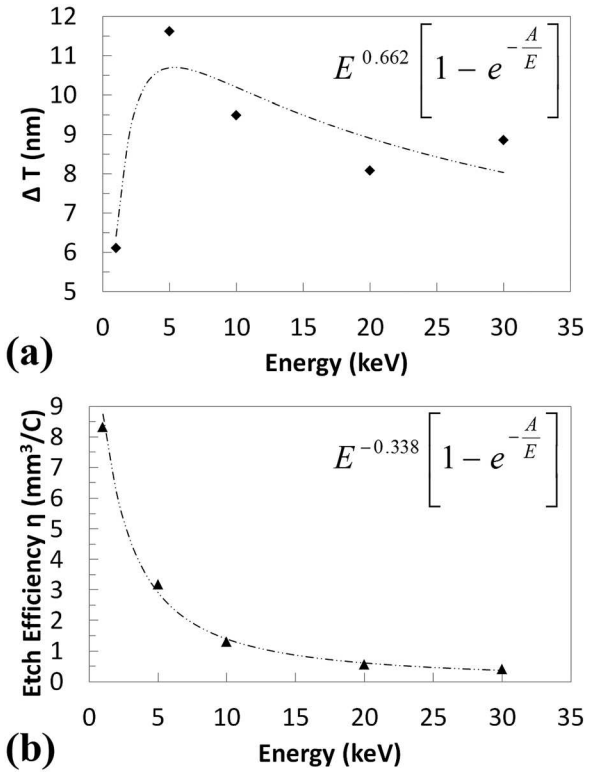

FIG. 3. Energy dependencies of (a) ΔT and (b) etch efficiency η. Sample was 63 nm 950k PMMA on Si, exposed at doses proportional to energy, no development. Base dose = 73.3 μC/cm^2 at 1 keV. In the fit formula, $\alpha = 0.66$ and A = 4.17 eV.

show that dose is a very important parameter for the thickness reduction effect. We can see that ΔT increases with dose to a certain level and then tends to saturate. As for the etch efficiency η, it decreases with decreasing dose. Another point we noticed from the results is that higher doses led to a smoother surface.

The effect of exposure energy is shown in Fig. 3. The results for ΔT are at constant dose factor, so the higher energy results correspond to proportionately higher dose reflecting the lower exposure sensitivity. The height difference first increases dramatically from 1 keV to ~5 keV and then decreases with energy beyond that value. Clearly, at low energy the thickness reduction mechanism is very efficient and increases strongly with dose. However, at higher energies, less impact occurs in the resist and most of the electrons penetrate deeply into the substrate, thereby reducing the impact of the beam. The etch efficiency; however, showed a very smooth and consistent trend, which is monotonically decreasing with energy. The reduction in etch efficiency is quite dramatic from 1 to ~5 keV reflecting the clear importance of low energy on a per electron basis.

Also included on these plots is a semiempirical formula to fit the experimental results. The form stems from the probability of an inelastic collision occurring within the resist per electron $(1 - e^{-N\sigma t})$, where $\sigma \sim 1/E$ is the inelastic collision cross section and E is the energy,[7,8] multiplied by the dose dependence of the etch result, which from Fig. 2(a) appears to be a power law with $\Delta T \sim (\text{dose})^{\alpha}$. As in this experiment exposure dose is proportional to energy E, the resulting formula becomes $\Delta T \sim E^{\alpha}(1 - e^{-A/E})$, where the parameters were fitted experimentally. The fit captures the overall behavior for ΔT and is also quite accurate for the etch efficiency. This suggests that electron collisions and the resulting fragmentation is the dominant factor for thickness reduction, rather than energy deposition, which would favor an evaporation mechanism.

Last, we have observed that both height difference and etch efficiency increase roughly in proportion to initial film thickness as shown in Fig. 4. If a surface dominated process, such as electron beam evaporation, was the main factor behind thickness reduction, then a strong resist thickness dependence would not be expected. The linear behavior evident in Fig. 4(a) supports a mechanism that depends on fragmentation throughout the volume, such as production of volatile fragments.

B. Postexposure processing

The above-presented results show that exposure conditions can be adjusted to increase the magnitude of the resist thickness reduction with values up to 32% demonstrated so far. However, it is unlikely that we will be able to reach clearance by exposure alone. Therefore, we proceeded with some postprocessing techniques to try to reach total clearance. We considered two approaches: heating and RIE. As discussed earlier, the concept was that heating will drive off volatile fragments remaining after electron exposure. For

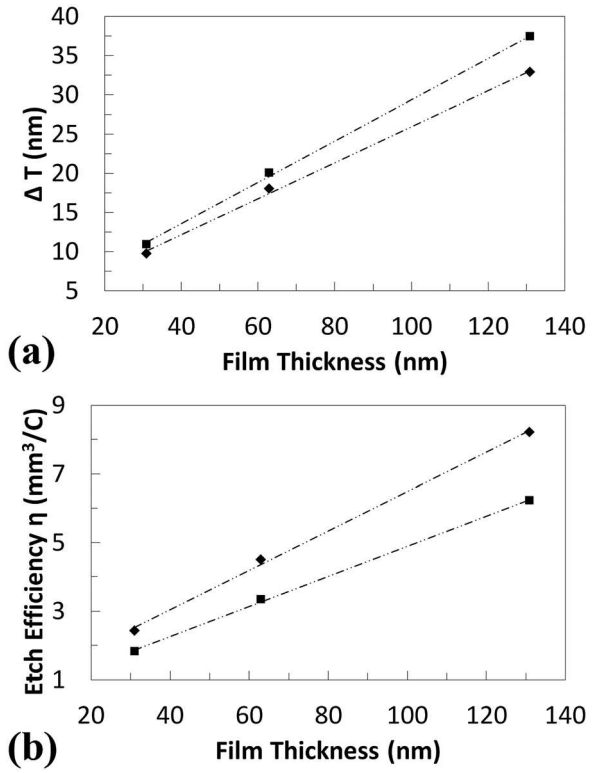

FIG. 4. Initial film thickness dependencies of (a) ΔT and (b) etch efficiency η. Sample was 950k PMMA on Si, exposed at 3 keV, no development. Diamonds: 400 μC/cm^2; squares: 600 μC/cm^2.

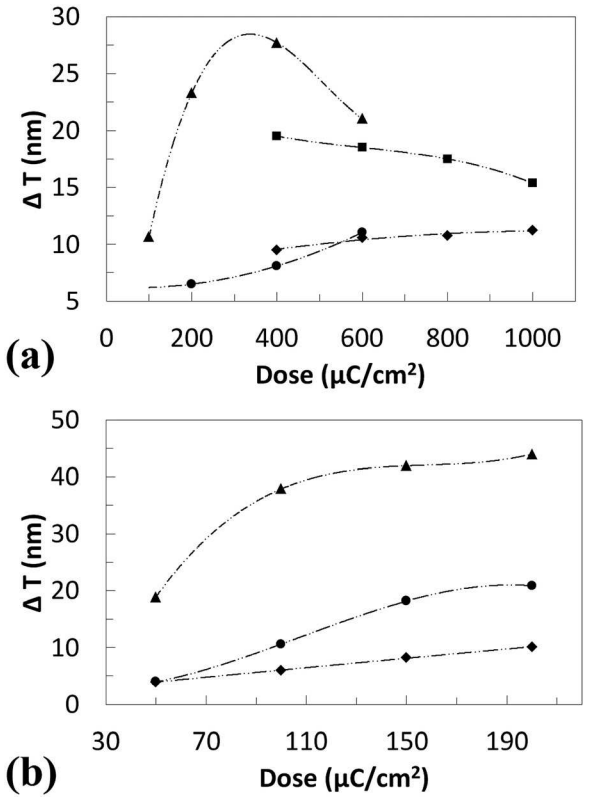

FIG. 5. Heating studies of ΔT for (a) 950k PMMA on Si, 33 ± 2 nm, exposed at 3 keV, no development. Diamonds: nonheated; circles: 47.5 °C for 1 min; triangles: 105 °C for 1 min; squares: 282 °C for 30 min (b) ZEP 520A on Si, 78 nm, exposed at 3 keV, no development. Diamonds: nonheated; circles: 75 °C for 30 s; triangles: 100 °C for 1 min.

RIE, we simply wish to preserve the already established height difference while reducing the exposed thickness to zero. Under ideal circumstances, the fragmented exposed region would etch more quickly than the unexposed region, thereby enhancing the height difference. This enhancement could be offset by a toughening in the exposed region due to cross-linking by usage of higher dose. We incorporated ZEP into these experiments because it provides better etch resistance yet shares some similarities with PMMA in terms of chemical composition.

The heating results for thickness are shown in Fig. 5 for several different temperatures as a function of dose. For PMMA resist, little effect of heating was observed for 47.5 °C compared with the unheated result. When the temperature increased to 105 °C, height difference was increased dramatically in the lower dose regime. Around the 400 μC/cm^2 dose, almost complete clearance was achieved. Beyond this dose, the curve began to drop again, presumably the result of cross-linking in the polymer during exposure. When the temperature increased even higher to 282 °C with extended baking time, heating was not as effective as it was at 105 °C. This is probably due to the cross-linking or other chemical changes of the PMMA during heating. As for ZEP, the results also demonstrated the effectiveness of heating, particularly at 100 °C. It is likely that, with some optimization, complete clearance is also possible with ZEP.

One concern of heating, especially at very high temperatures, is reflow and distortion of the pattern as demonstrated in Fig. 6. Figure 6(a) shows the profile for exposed but unheated PMMA. Although clearance was not reached, the thickness reduction was more than 33% of the initial film thickness. Figure 6(b) shows the result after heating at 105 °C for 1 min. Note that the dose of Fig. 6(b) was 600 μC/cm^2, which was lower than the doses of Figs. 6(a) and 6(c). Nevertheless, ΔT was 21 nm, ~60% of the initial film thickness. We began to see some reflow induced distortion but still moderate. Figure 6(c) shows the result after annealing at 282 °C for 30 min. The distortion due to the reflow is clear. Also, we observed that clearance was achieved for the partially exposed areas around the perimeter of the exposed squares, where the height difference is ~31 nm. However, we noticed that there were 5–6 nm tall 1 μm^2 squares formed in the center of the heated sample. We believe this may be due to the cross-linked or carbonized PMMA[9] as a result of a long duration high temperature baking. Finally, as these two samples were exposed at exactly the same conditions, we could also conclude that there is an interaction between heating and dose. Based on the results we have obtained, we believe that heating is more effective in lower dose regimes up to about 400 μC/cm^2 with heating temperatures near 100 °C.

The RIE results for thickness are shown in Fig. 7. Immediately after the exposure, the sample had a film thickness of 106 nm with $\Delta T = 38$ nm. After the cryo-etch, film thickness was reduced to 34 nm with $\Delta T = 20$ nm. Note that ΔT was reduced too. This means that the exposed region was etched

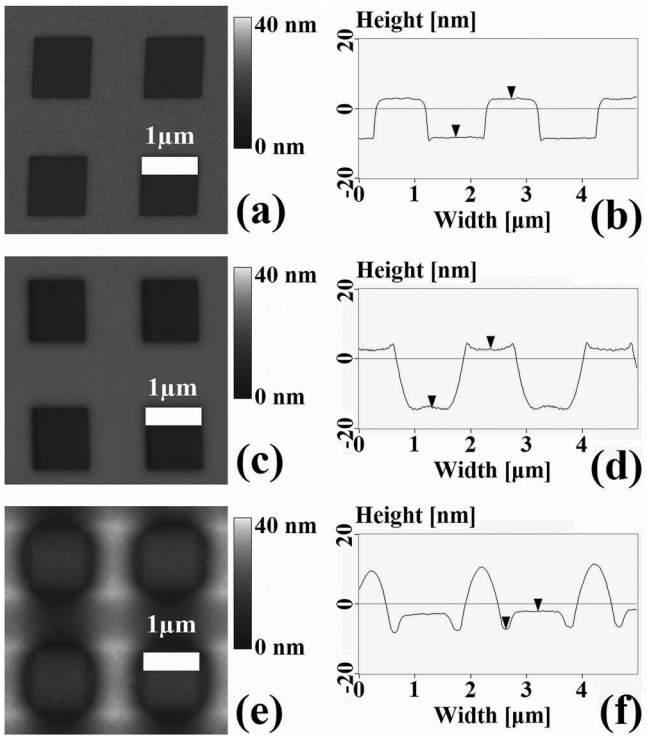

FIG. 6. Comparison of no heating vs heating processes. All samples were 950k PMMA on Si, exposed at 3 keV. Top view and cross-section view, respectively. (a, b) Initial film thickness = 31 nm, 1000 μC/cm^2, no heating, $\Delta T = 11$ nm. (c, d) Initial film thickness = 35 nm, 600 μC/cm^2, 105 °C for 1 min, $\Delta T = 21$ nm. (e, f) Initial film thickness = 31 nm, 1000 μC/cm^2, 282 °C for 30 min, $\Delta T = 15$ nm. Squares in the center are 5–6 nm in height.

slower than the unexposed region. As mentioned earlier, the reason could be that the exposed region was hardened by resist cross-linking. We also noticed that there were small pieces of PMMA redeposited on the surface after RIE. A possible solution would be to add another de-scum procedure after the etching is done. Although in our experiments, normal RIE process does not have this issue, we believe that cryo-etch is a better process than normal RIE. A major reason is that cryo-etch could maintain the established height difference better than the normal RIE. We compared two samples exposed under the same conditions ($\Delta T = 38$ nm), but subjected to different RIE processes. For the sample that went through the normal RIE process, ΔT decreased to 13 nm; however, for the sample that went through the cryo-etch process, ΔT decreased to 20 nm.

We have also obtained a dose dependency for the cryo-etch process, as shown in Fig. 8. It seems that ΔT tends to be slightly higher at approximately 400 μC/cm^2. This is consistent with the optimum heating dose value [see Fig. 5(a)], which may suggest that the molecular mechanisms of scission and/or cross-linking in PMMA are dose dependent and undergo changes at ~400 μC/cm^2 for 3 keV exposure.

Presently, this is an early stage research. Many parameters can be optimized in future experiments. Based on the observations we had, we believe the exposure dose should be reduced to about 400 μC/cm^2 if 3 keV is used. As for the RIE conditions, at this stage, further study is needed to find out whether ion sputtering etch or reactive ion chemical etch should be the principal process during the RIE, as well as how to balance these two processes. Through co-optimization with the exposure conditions, we expect to achieve total clearance with RIE.

C. High resolution trials

The work described previously was performed on 1 μm size patterns. These dimensions were appropriate to perform AFM measurements, but are not representative of the typical length scales used for EBL. Hence, we have also performed high resolution work assessed by SEM. On both PMMA and ZEP resist, we are able to pattern 70 nm half-pitch gratings as shown in Fig. 9. (Higher magnification images were not achieved due to modification of the sample by the electron

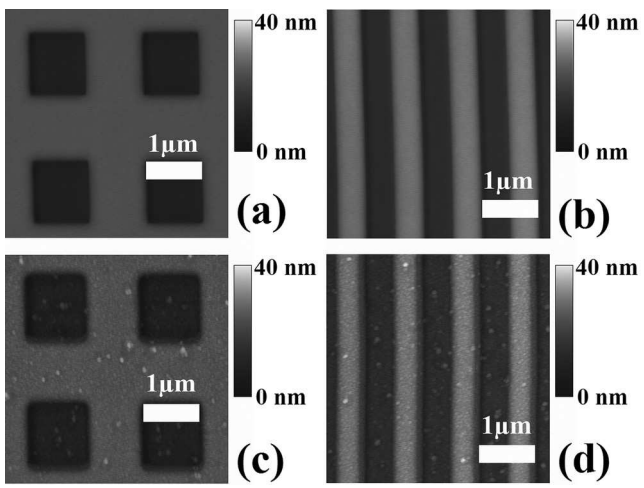

FIG. 7. AFM images of preliminary RIE results. 950k PMMA on Si, exposed at 3 keV, 1000 μC/cm^2, no development. 1 μm squares and 500 nm lines with 500 nm spacings, respectively. (a,b) Before ICPRIE, initial film thickness = 106 nm, $\Delta T = 38$ nm. (c,d) After ICPRIE at −110 °C, de-scum at 5 mTorr, $O_2 = 20$ sccm, ICP = 150 W, rf = 20 W, 5 s, etching at 7.5 mTorr, SF_6:O_2 = 45:10 sccm, ICP = 400 W, rf = 6 W, 60 s, film thickness = 34 nm, $\Delta T = 20$ nm.

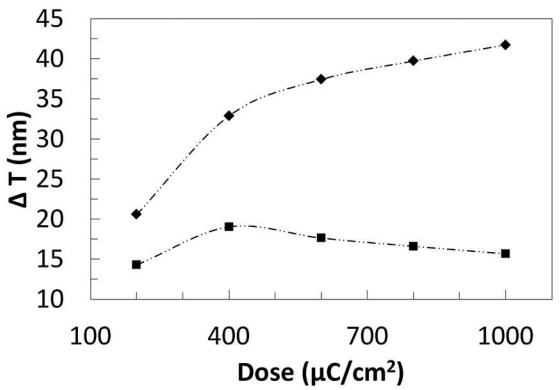

FIG. 8. Dose dependency of ΔT in ICPRIE. Sample was 131 nm 950k PMMA on Si, exposed at 3 keV with no development. Diamonds: ΔT before the cryo-etch; Squares: ΔT after the cryo-etch. ICPRIE was performed at −110 °C, de-scum at 5 mTorr, $O_2 = 20$ sccm, ICP = 150 W, rf = 20 W, etching at 7.5 mTorr, SF_6:O_2 = 45:10 sccm, ICP = 400 W, rf = 6 W. The process comprised 10 s de-scum and 60 s etch followed by another 10 s de-scum and 30 s etch.

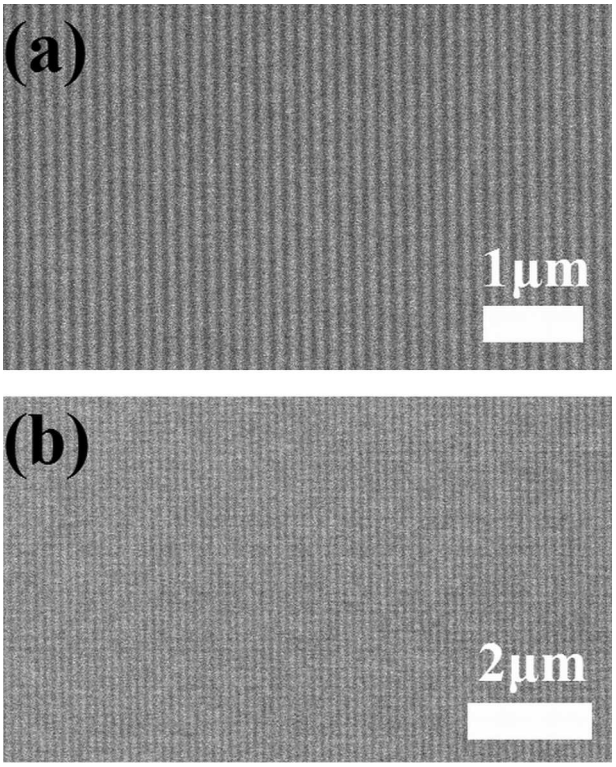

FIG. 9. SEM images of 70 nm half-pitch gratings exposed at 3 keV, 7.5 μm aperture, no development, on (a) 72 nm 950k PMMA on Si, ~600 μC/cm^2 (b) 64 nm ZEP 520A on Si, ~100 μC/cm^2.

beam during SEM imaging.) Although the samples have likely not cleared down to the substrate, the contrast modulation observed does indicate that the thickness reduction is scalable to high resolution structures. Further work on cross-sectional images would be necessary to confirm this.

IV. SUMMARY AND CONCLUSIONS

The purpose of the work presented in this paper is to utilize the natural resist thinning due to electron beam irradiation and investigate a patterning approach without the usage of liquid development. We have employed heating and RIE as postexposure processes in order to increase resist thinning and obtain pattern clearance. Even without any postexposure processing, we have observed substantial resist thickness reduction of 32% by electron beam irradiation. This reduction is likely due to production of volatile fragments through the scission process in the resist. The thickness reduction induced by electron beam irradiation depends on exposure dose, beam energy, and initial resist film thickness. The doses required for this process are higher than typical exposure doses used in standard liquid development processes. Low exposure energy is particularly important in achieving this result. Postexposure heating can increase the height difference and even achieve clearance; however, at the risk of pattern distortion. The effectiveness of postexposure heating is likely due to the evolution of less volatile fragments. There is an interaction between heating and dose, probably through cross-linking and carbonization behavior. To date, we are able to pattern 70 nm half-pitch gratings on both PMMA and ZEP without liquid development. Further optimization of both exposure and postprocessing is possible, with good prospect for a viable EBL patterning process that does not require liquid development.

ACKNOWLEDGMENTS

This work was supported by the Natural Sciences and Engineering Research Council of Canada (NSERC) and the National Institute for Nanotechnology (NINT). Finally, the authors would like to acknowledge technical support of the University of Alberta Nanofab, University of Alberta Integrated Nanosystems Research Facility and the NINT Electron Microscopy Group.

[1]H. Koop, M. Zech, K. Karrai, D. Schnurbusch, M. Müller, T. Gründl, M.-C. Amann, and A. W. Holleitner, J. Vac. Sci. Technol. B **28**, 802 (2010).
[2]M. Kotera and Y. Akiba, Jpn. J. Appl. Phys. **49**, 06GE08 (2010).
[3]N. Arjmandi, L. Lagae, and G. Borghs, J. Vac. Sci. Technol. B **27**, 1915 (2009).
[4]N. Vourdas, A. G. Boudouvis, and E. Gogolides, J. Phys.: Conf. Ser. **10**, 405 (2005).
[5]C. Zhang, C. Yang, and D. Ding, Appl. Surf. Sci. **227**, 139 (2004).
[6]H. Nabesawa, T. Hitobo, S. Wakabayashi, T. Asaji, T. Abe, and M. Seki, Sensors Actuators B **132**, 637 (2008).
[7]M. Aktary, M. Stepanova, and S. K. Dew, J. Vac. Sci. Technol. B **24**, 768 (2006).
[8]B. Wu and A.R. Neureuther, J. Vac. Sci. Technol. B **19**, 2508 (2001).
[9]H. Duan, J. Zhao, Y. Zhang, E. Xie, and L. Han, Nanotechnology **20**, 135306 (2009).